Original Article

Inhibition of hepatocellular carcinoma progression by artesunate via modulation of the TLR4/MyD88/NF-κB signaling pathway

Yongchao Wu[1], Jianhua Wu[2], Zhigang Li[1], Zhonglin Wu[1], Shunzong Li[1], Guang Yang[1], Xiaocui Rong[1], Qi Wang[3], Yazhou Li[1], Qingqing Xia[1], Gaofeng Shi[3]

[1]Department of Radiology, The Fourth Hospital of Hebei Medical University, Shijiazhuang, China; [2]Animal Center, The Fourth Hospital of Hebei Medical University, Shijiazhuang, China; [3]Department of CT/MRI, The Fourth Hospital of Hebei Medical University, Shijiazhuang, China

Contributions: (I) Conception and design: Y Wu, J Wu; (II) Administrative support: G Shi; (III) Provision of study materials or patients: Z Li, Z Wu, S Li, G Yang; (IV) Collection and assembly of data: X Rong, Q Wang, Y Li; (V) Data analysis and interpretation: Q Xia; (VI) Manuscript writing: All authors; (VII) Final approval of manuscript: All authors.

Correspondence to: Gaofeng Shi, MD. Department of CT/MRI, The Fourth Hospital of Hebei Medical University, 12 Jiankang Road, Shijiazhuang 050011, China. Email: gaofengs62@sina.com.

Background: Liver cancer remains a frequent cause of cancer-related death, and thus targeted drugs urgently need to be developed. Artesunate (ART) inhibits the progression of liver cancer; however, its mechanism of action remains unclear. The primary aim of this study is to clarify whether ART inhibits the progression of hepatocellular carcinoma (HCC) cells by suppressing the Toll-like receptor 4 (TLR4)/MyD88/nuclear factor (NF)-κB pathway.

Methods: *In vitro* studies demonstrated the effects on cell proliferation, invasion, and migration through a series of phenotypic experiments. Specifically, the CCK8 was used to assess the impact on cell proliferation, while the Transwell assay was employed to evaluate the effect on cell invasion. A xeno-inhibitory tumor model was established *in vivo* to verify the therapeutic effects of ART. Western blotting was used to detect changes in the TLR4/MyD88/NF-κB pathway.

Results: The study showed that ART inhibits HCC cell proliferation, invasion, and migration and induces apoptosis in a dose-dependent manner. *In vivo* studies indicated shown that ART treatment in xenograft tumor models could consistently reduce tumor growth. Moreover, ART inhibited the viability, colony formation, migration, and invasion ability of HCC cells while promoting their apoptosis in a dose-dependent manner. The treatment of xenograft models with ART consistently reduced tumor growth. Furthermore, Western blot analysis demonstrated that the levels of TLR4 and its known downstream effectors (TRAF6, MyD88, and NF-κB) were markedly downregulated after ART treatment in Huh-7 and liposaccharide-stimulated Huh-7 cells.

Conclusions: These results indicate that ART has a potent effect on the development of HCC cells, the underlying mechanisms of which may be associated with alterations in the TLR4/MyD88/NF-κB signaling pathway in HCC. Therefore, further development of ART as a therapeutic agent is warranted.

Keywords: Artesunate (ART); hepatocellular carcinoma (HCC); Toll-like receptor (TLR); MyD88; nuclear factor-κB (NF-κB)

Submitted Feb 07, 2025. Accepted for publication Apr 17, 2025. Published online Apr 27, 2025.
doi: 10.21037/jgo-2025-95
View this article at: https://dx.doi.org/10.21037/jgo-2025-95

Introduction

In 2020, primary liver cancer was the sixth most commonly diagnosed cancer and the third leading cause of cancer-related death worldwide, with approximately 906,000 new cases and 830,000 deaths (1). More than half of hepatocellular carcinoma (HCC) cases are diagnosed at an advanced stage (2). Despite recent advances in the diagnosis and treatment of HCC, the overall prognosis remains dismal, with a 3-year survival rate of 12.7% and a median survival of 9 months (3). Sorafenib, a first-generation targeted tyrosine kinase inhibitor (TKI), improves the overall survival of patients with advanced HCC (4,5). Numerous patients with advanced HCC develop resistance to sorafenib during treatment and thus do not benefit from it in the long-term (6). Although several novel TKIs, including apatinib, lenvatinib, and regorafenib, have shown promising therapeutic effects in HCC, their application is limited due to acquired drug resistance and side effects (7,8). Therefore, curative therapeutic strategies for advanced HCC urgently need to be developed.

Artesunate (ART), a semisynthetic derivative of artemisinin, is an effective compound for treating malaria (9). The potential anticancer effects of ART have been confirmed in several tumors (9-11). Previous studies have revealed that ART exerts antitumor effects by mediating cell cycle arrest, inducing DNA damage, blocking angiogenesis, inhibiting metastasis, and promoting apoptosis (12-14). In addition, ART has been studied as both a combination drug and an inhibitor of drug resistance in HCC (11,15).

Highlight box

Key findings

- Artesunate (ART) can significantly inhibit the relative expression levels of MyD88, nuclear factor (NF)-κB, Toll-like receptor 4 (TLR4), and TRAF6 proteins and suppress the activation of the TLR4/MyD88/NF-κB signaling pathway.

What is known and what is new?

- ART can inhibit the proliferation, invasion and migration of hepatoma cells and induce the apoptosis of hepatoma cells.
- ART may exert an anticancer effect against liver cancer by mediating the TLR4/MyD88/NF-κB signaling pathway.

What is the implication, and what should change now?

- ART may be an effective drug for the treatment of liver cancer. A potential new anticancer mechanism of ART has been discovered, providing a theoretical basis regarding the role of ART as an inhibitor of the TLR4/MyD88/NF-κB signaling pathway.

Toll-like receptors (TLRs) are pattern recognition receptors. Toll-like receptor 4 (TLR4), a member of the TLR family, initiates innate immune or inflammatory responses (16). As a critical adapter protein for TLR4, MyD88 is bound to the Toll/interleukin-1 (IL-1) receptor (TIR) domain of TLRs; upon recognizing and connecting to IL-1 receptor-associated kinases and TRAF6, TLRs can be dislocated from nuclear factor (NF)-κB, eventually leading to NF-κB activation (17,18). The levels of several inflammatory cytokines are elevated following activation of the NF-κB pathway, including tumor necrosis factor (TNF)-α, IL-6, and IL-1β, mediating liver inflammation and tumorigenesis (19). A previous study demonstrated that hypoxia-inducible UPS13 contributes to HCC growth and metastasis by enhancing the TLR4/MyD88/NF-κB signaling pathway (20). Similarly, Baishouwu extract was found to suppress the initiation and progression of HCC by inhibiting the TLR4/MyD88/NF-κB signaling pathway (21). Overall, the TLR4/MyD88/NF-κB signaling pathway is critical in HCC development, but little is known about the actions of ART on the TLR4/MyD88/NF-κB signaling pathway-mediated antitumor response. Although ART has been identified as an inhibitor of TLR4 (22,23), it is unknown whether ART can also act as a TLR4 inhibitor in liver cancer, and the mechanism between TLR4 signal transduction and lipopolysaccharide (LPS) is poorly understood. Therefore, the primary aim of this study was to clarify the mechanism by which ART exerts a therapeutic effect in liver cancer. We present this article in accordance with the ARRIVE and MDAR reporting checklists (available at https://jgo.amegroups.com/article/view/10.21037/jgo-2025-95/rc).

Methods

Cell culture

Human normal liver cells THLE-2, along with HCC cells Huh-7, SNU-182, HLE, C3A, and HepG2 (HepG2 is also referred to as the hepatoblastoma cell line) (24,25) were purchased from Procell (Procell Life Science & Technology Co., Ltd., Wuhan, China). All the cells were cultured in 10 - cm dishes (cat. no. FCD100; Beyotime Biotechnology, Shanghai, China) without any special coating treatment. Human liver normal cells and HCC cells were cultured in Dulbecco's Modified Eagle Medium (DMEM; Gibco, Thermo Fisher Scientific, Waltham, MA, USA) supplemented with 10% fetal bovine serum (FBS) (Gibco)

in a humidified incubator containing 5% CO_2 at 37 ℃. ART [MedChem Express (MCE), Monmouth Junction, NJ, USA] was dissolved in dimethylsulfoxide (DMSO; Sigma-Aldrich, St. Louis, MO, USA) and stored in the dark. The final dilution of DMSO was less than 0.2%.

Cell viability assay

The effects of ART on Huh-7 and SNU-182 cell viability were examined using cell counting kit-8 (CCK-8) according to the manufacturer's instructions (Dojindo Laboratories, Kumamoto, Japan) (26). Briefly, Huh-7 and SNU-182 cells in the logarithmic growth phase were seeded into 96-well microplates at a density of 1×10^3 cells per well and treated with ART (0, 20, 40, or 80 μg/mL). Huh-7 cells were treated with 10 μg/mL of LPS (MCE) for 72 h. At each time point (0, 24, 48, and 72 h), 10 μL of diluted CCK-8 was added into each well, and cells were incubated in a 5% humidified CO_2 incubator for 2 h at 37 ℃. Absorbance was measured at 450 nm with a microplate reader (Bio-Tek Instruments, Winooski, VT, USA).

Cell counting

Treat Huh-7, SNU-182 and HepG2 cells with ART (40 μg/mL) for 72 h. For the control group, do not add ART and incubate normally for 72 h. After the incubation, add 2 mL of 0.25% trypsin digestion solution (cat. no. C0203; Beyotime Biotechnology, Shanghai, China) to the HCC cells and incubate for 2 min. Subsequently, add 3 mL of DMEM medium, collect the cell suspension, and transfer it into a centrifuge tube. According to the requirements of the Cell Viability Detection Kit (cat. no. C0011; Beyotime Biotechnology, Shanghai, China), add trypan blue for staining. Then, place the sample in a cell counter to calculate the number of cells.

Colony formation assay

Cells were seeded in six-well plates at a density of 500 cells/well. After 24 h of incubation, the cells were treated with different doses of ART for 10–12 days. The cells were washed three times with phosphate-buffered saline (PBS), fixed with methanol for 15 min, and stained with a 0.5% crystal violet solution for 10 min. Clones were considered viable if they contained >50 cells. The corresponding photographs were captured.

Wound-healing assay

For the wound-healing assay, a 10-μL pipette tip was used to create a straight, uniform linear scratch across the cell monolayer, which was followed by a gentle wash with PBS to remove cellular debris. The wound closure was photographed under an inverted microscope (Nikon, Tokyo, Japan) at 0, 24, and 48 h after ART. Each scratch was analyzed, and cell migration rates were calculated as described previously (27). Each experiment was repeated three times.

Cell invasion assay

The tumor cell invasion assay was performed in a 24-well Transwell chamber (Corning, Corning, NY, USA), which contained an 8-μm pore size polycarbonate membrane filter with Matrigel (BD Biosciences, Franklin Lakes, NJ, USA). Briefly, 2×10^5 cells were placed in the upper chambers and incubated in 200 μL of serum-free medium with 0, 20, 40, or 80 μg/mL ART, while 500 μL of medium with 10% FBS was added in the lower chambers. After 24-h culturing in a 5% CO_2 humidified incubator at 37 ℃, cells on the upper side of the membrane filters were removed, and cells on the lower side were fixed in methanol and stained with 0.1% crystal violet. The stained cells were defined as migrating cells and counted under a microscope. The cells on the lower side of the membrane filters were defined as invasive cells and counted in five random fields for each membrane filter.

Quantitative polymerase chain reaction

Extract the exponentially-growing HCC cells. Add 2 mL of 0.25% trypsin digestion solution (cat. no. C0203; Beyotime Biotechnology, Shanghai, China) and incubate the HCC cells for 2 min. Subsequently, add 3 mL of DMEM medium, collect the cell suspension, and transfer it into a centrifuge tube. Prepare the reaction system according to the requirements of the cDNA synthesis kit (cat. no. D7170L; Beyotime Biotechnology, Shanghai, China). Incubate it at 42 ℃ for 60 min for the reverse transcription reaction. Subsequently, incubate at 80 ℃ for 10 min to inactivate the reverse transcriptase, and then place it on ice. Exponentially grown liver cancer cells were extracted, and cell digestion was performed as described above. The cells were then centrifuged at 1200 g for

3 min. An appropriate amount of TRIzol solution (cat. no. R0016l; Beyotime Biotechnology, Shanghai, China) was added, and total RNA was extracted according to the manufacturer's instructions. The BeyoFast SYBR Green quantitative polymerase chain reaction (qPCR) mixture was added to the premix (cat. no. D7262; Beyotime Biotechnology). The template DNA was preheated at 95 ℃ on the polymerase chain reaction (PCR) apparatus for 3 min, completely denatured, and then entered into the amplification cycle. In each cycle, the template remained denatured at 95 ℃ for 35 s, and then the temperature was reduced to 65 ℃ for 30 s, allowing the primer and template to be fully annealed. The template was held at 74 ℃ for 1 min, the primer was made to extend to the template, the DNA was synthesized, the cycle was repeated 39 times, and the system was finally set to 4 ℃ permanently. A 7900HT fluorescent quantitative PCR instrument (cat. no. 4351405; Thermo Fisher Scientific, Waltham, MA, USA) was set according to the above instructions. The data were statistically analyzed using Graph Prism 9.5.0 software (GraphPad Software, San Diego, CA, USA). The primer information is detailed in Table S1. The amplified products were confirmed to be the expected ones through PCR gel electrophoresis. Moreover, all experiments were carried out three times independently.

Quantification of cell apoptosis

Apoptosis was evaluated using a phycoerythrin-conjugated Annexin V/7-AAD apoptosis detection kit (BD Biosciences). The cells were treated with different doses of ART for 48 h in six-well plates, harvested, and washed two times with cold PBS. Cells were stained with Annexin V and 7-AAD in a binding buffer for 15 min in the dark at room temperature. Apoptosis was quantified using a FACSCalibur flow cytometer (BD Biosciences) (28). Each experiment was repeated three times.

In vivo xenograft models

Four-week-old male BALB/c nude mice were purchased from SPF (Beijing) Biotechnology Co. Ltd. (Beijing, China; permission no. SCXK [Jing] 2019–0010). The mice were housed in a specific pathogen-free environment at the Laboratory Animal Center of the Fourth Hospital of Hebei Medical University. All the animal experiments were approved by the Institutional Animal Care and Ethics Committee of the Fourth Hospital of Hebei Medical University (No. 2021028; approval date: July 21, 2021). These experiments complied with the "Regulations on the Administration of Laboratory Animals" and the "Guidelines for the Review of Laboratory Animal Welfare and Ethics" issued by the Ministry of Science and Technology of the People's Republic of China for the care and use of animals. A protocol was prepared before the study without registration. Huh-7 cell suspension (5×10^6 cells/mouse in 200 µL of PBS) was subcutaneously injected into the right flanks of each mouse. The mice were randomly divided into four groups (six mice/group), and ART was delivered by intragastric administration when the average volume of the tumors grew to approximately 100–200 mm^3. The negative control was treated with PBS, while the three ART drug therapy groups received 50, 100, and 200 mg/kg of ART. PBS and ART were administered intragastrically daily for 4 weeks. The tumor volume was measured and calculated (long diameter × short diameter^2 × 0.5) every 7 days (29). The initial gas concentration of isoflurane (cat. no. R510-22-10; RWD Life science, Shenzhen, China) introduced using a gas anesthesia machine (Anhui Zhenghua Biologic Apparatus Facilities, Huaibei, China) was 3–4%, and the maintenance anesthesia concentration of isoflurane was 1.5–2%. The mice were placed in the *in vivo* imaging system for observation. An *in vivo* imaging system was used to observe the growth of the subcutaneous tumor cells. Before observation, each mouse was intraperitoneally injected with 150 µL of 30 mg/mL fluorescein substrate (cat. no. HY-12591AMCE). *In vivo* imaging was performed 10 to 25 min after injection. After the imaging was complete, the mice were killed via inhalation of CO_2 (60% vol/min). The cessation of breathing, cessation of heartbeat, fixed and dilated pupils were considered to indicate the death of mice, with a 5-minute period of CO_2 inhalation maintained prior to these observations.

Western blot analysis

After treating with different doses of ART for 3 days, the cells in the control group were left untreated. Then, Huh - 7 cells from each group were collected and homogenized in RIPA lysis buffer (Sigma - Aldrich) containing protease inhibitors. Proteins were separated using sodium dodecyl sulfate-polyacrylamide gel electrophoresis (SDS-PAGE) and transferred onto polyvinylidene difluoride membranes (Roche, Basel, Switzerland). After being blocked with 5% nonfat dried milk for 2 h, the membrane was incubated with primary antibodies at 4 ℃ overnight, which was

followed by the incubation with horseradish peroxidase (HRP)-conjugated secondary antibody (1:5,000 dilution; Thermo Fisher Scientific) for 2 h. The protein bands were visualized using an enhanced chemiluminescence (ECL) chemiluminescence system (Alpha InnoTec, Kasendorf, Germany) and quantitatively analyzed (30). Calculate the ratio of the target protein to the internal reference protein. Normalize the data with the control group as the benchmark. Conduct three independent experiments. Present the results as the mean ± standard error of the mean (SEM) to ensure the reproducibility of the results. The antibodies used for Western blot, including TLR4 (1:1,000 dilution; cat. no. AF7017), TRAF6 (1:1,000 dilution; cat. no. AF5376), MyD88 (1:1,000 dilution; cat. no. AF5195), NF-κB (1:1,000 dilution; cat. no. BF8005), β-actin (1:1,000 dilution; cat. no. AF7018), goat anti-rabbit (1:10,000 dilution; cat. no. S0001), and goat anti-mouse (1:10,000 dilution; cat. no. S0002), were obtained from Affinity Biosciences (Cincinnati, OH, USA) and were used to detect specific proteins in the Western blot analysis.

Statistical analysis

All experiments were ensured to be conducted three times independently. The data are presented as mean ± standard deviation (SD). A Student *t*-test was performed to analyze the results of the CCK-8, colony formation, migration, invasion, apoptosis, and nude mouse xenograft assays. $P<0.05$ was considered to indicate statistically significant differences. All the statistical analyses were performed using SPSS version 19.0 software (IBM Corp., Armonk, NY, USA).

Results

ART inhibited cell viability in human HCC cells

The two-dimensional (2D) and Three-dimensional (3D) molecular structural formulas of ART are shown in *Figure 1A*. The results of CCK8 showed that ART inhibited the proliferation of Huh-7, SNU-182, and HepG2 cells in a dose-dependent manner. The half-maximal inhibitory concentration (IC_{50}) of Huh-7 was 49.18 μg/mL, that of SNU-182 was 46.11 μg/mL, and that of HepG2 was 73.62 μg/mL (*Figure 1B*). Among them, ART at a concentration of 5 μg/mL had no significant effect on the viability of HCC cells. After treatment with ART (40 μg/mL), the morphology of Huh-7 and SNU-182 cells included a smaller size, and the number of cells decreased significantly. Meanwhile, although the effect on HepG2 cell morphology was minimal, the number of HepG2 cells did decrease (*Figure 1C,1D*). This may be related to the expression of TLR4 in HepG2. We observed that Huh-7 and SNU-182 cells had the highest levels of TLR4 messenger RNA (mRNA) expression in five different HCC cell lines compared to those in normal hepatocytes (*Figure 1E*). Meanwhile, the mRNA level of TLR4 in HepG2 was the lowest compared with that in the other hepatoma cell lines. We speculate that this may be the reason why ART has no effect on the morphology of HepG2 cells. Therefore, we selected Huh-7 and SNU-182 cells, as they exhibited a relatively obvious effect of ART on liver cancer cells and a high expression of TLR4. To further verify the impact of ART on the cell proliferation ability, we further confirmed the inhibitory effect of ART on the proliferation of HCC cells through the colony-formation assay (*Figure 1F*).

ART suppressed the migration and invasion of HCC cells

Wound-healing assays were performed to determine the migratory abilities of Huh-7 and SNU-182 cells. ART decreased the migration capacity as compared to that in the control group (*Figure 2A*). In the Transwell assay, ART treatment dramatically inhibited Huh-7 and SNU-182 cell invasion (*Figure 2B*). These findings suggest that ART inhibits the migration and invasion of HCC cells.

Art inhibited HCC cell growth via cell apoptosis

ART inhibited Huh 7 and SNU-182 cell viability in a concentration- and time-dependent manner (*Figure 3A*). Flow cytometry was performed to assess the apoptosis rate in Annexin V/7-AAD double-stained Huh-7 and SNU-182 cells. As shown in *Figure 3B*, apoptotic cells significantly increased after treatment with ART for 48 h ($P<0.05$). Thus, apoptosis may be involved the inhibition of HCC cell growth that is induced by ART.

ART inhibited the growth of Huh-7 cells in vivo

The Huh-7 cell xenograft model was used to evaluate the *in vivo* effects of ART. The volume of Huh-7 xenografts in mice treated with ART was smaller than that in mice treated with PBS at 14, 21, and 28 days after implantation (*Figure 4A,4B*). Similar results were demonstrated by the

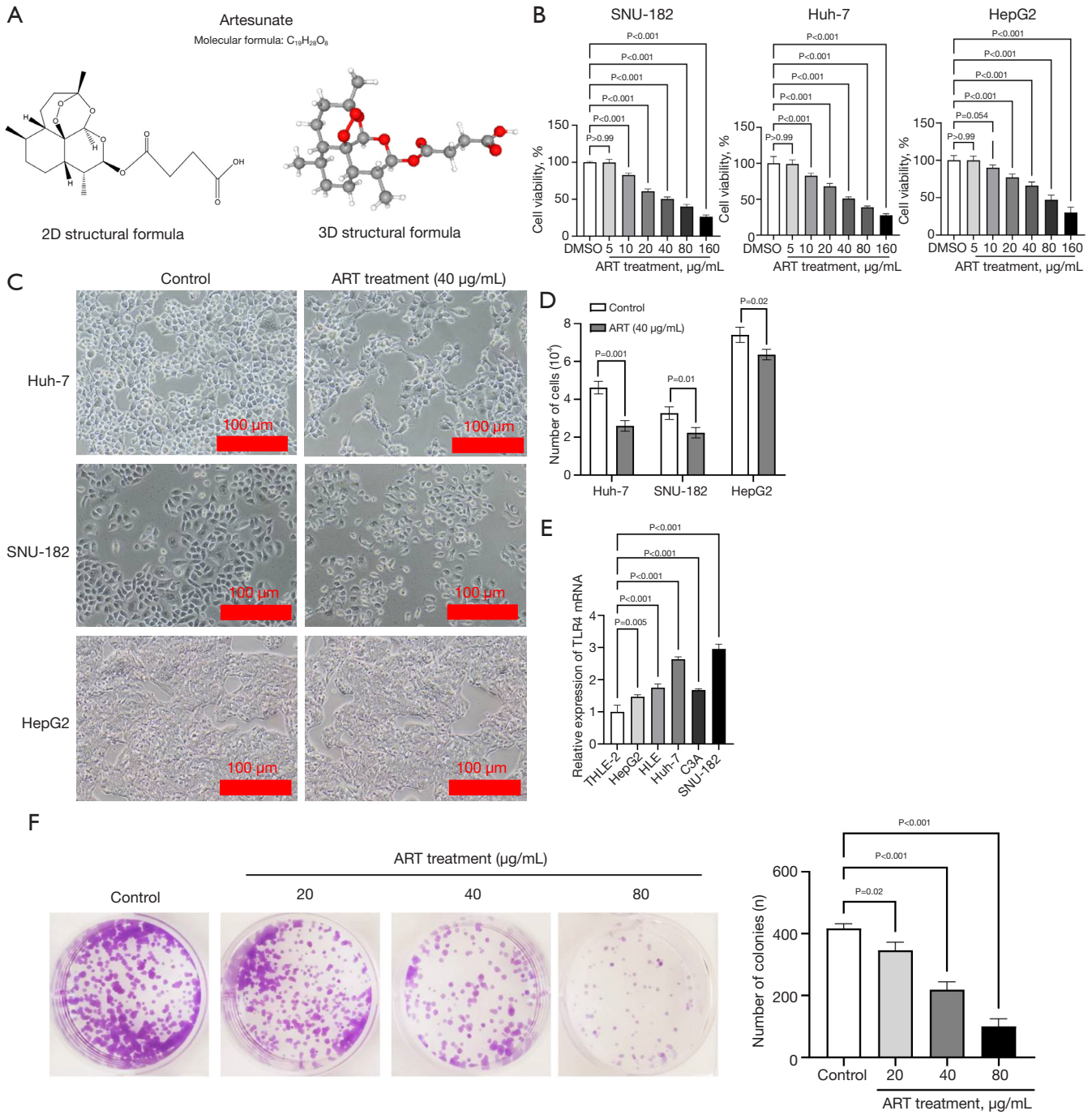

Figure 1 Effects of ART on the viability and colony formation of HCC cells. (A) ART 2D and 3D molecular structure formulae. (B) The changes in cell viability of Huh-7, SNU-182, and HepG2 cells treated with ART for 48 h were detected using CCK8. (C,D) Observe the morphological changes of Huh-7 and SNU-182 HCC cells treated with ART (40 μg/mL) through a microscope. Then, calculate the changes in the number of viable cells by trypan blue staining. (E) The expression level of TLR4 mRNA in ART-treated THLE-2, HepG2, HLE, Huh-7, C3A, and SNU-182 cells was detected using qPCR after 48 h. (F) ART suppression of Huh-7 cell colony formation was demonstrated via a colony formation assay (stained with 0.5% crystal violet). 2D, two-dimensional; 3D, three-dimensional; ART, artesunate; CCK8, cell counting kit-8; HCC, hepatocellular carcinoma; qPCR, quantitative polymerase chain reaction; TLR4, Toll-like receptor 4.

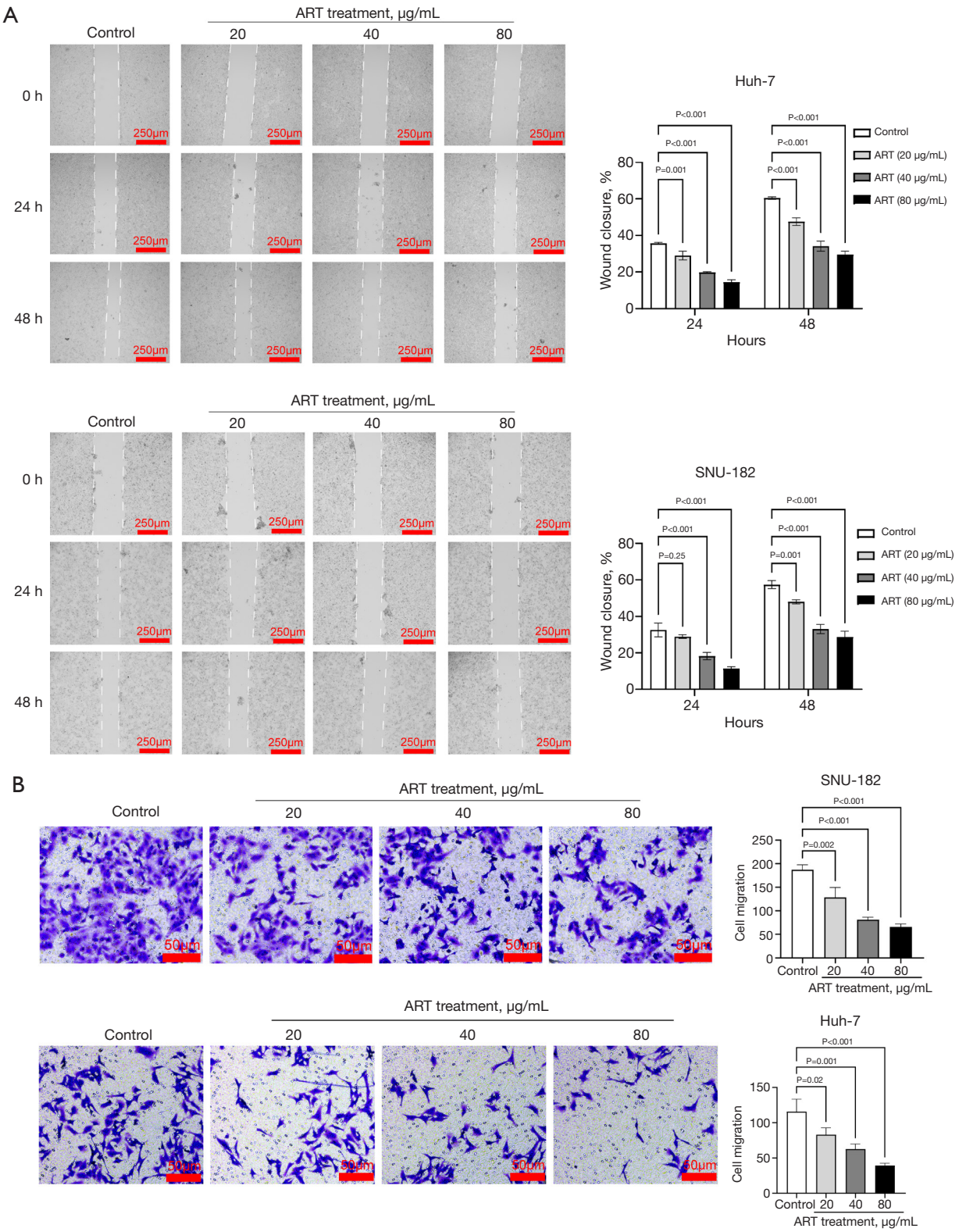

Figure 2 ART could inhibit the invasion and migration abilities of hepatoma cells Huh-7 and SNU-182. (A) The cell migration ability of Huh-7 and SNU-182 cells was detected by cell scratch assay at 0 h, 24 h and 48 h under different concentrations of ART. (B) The invasion ability of Huh-7 and SNU-182 cells was detected by the Transwell method and stained with 0.5% crystal violet. ART, artesunate.

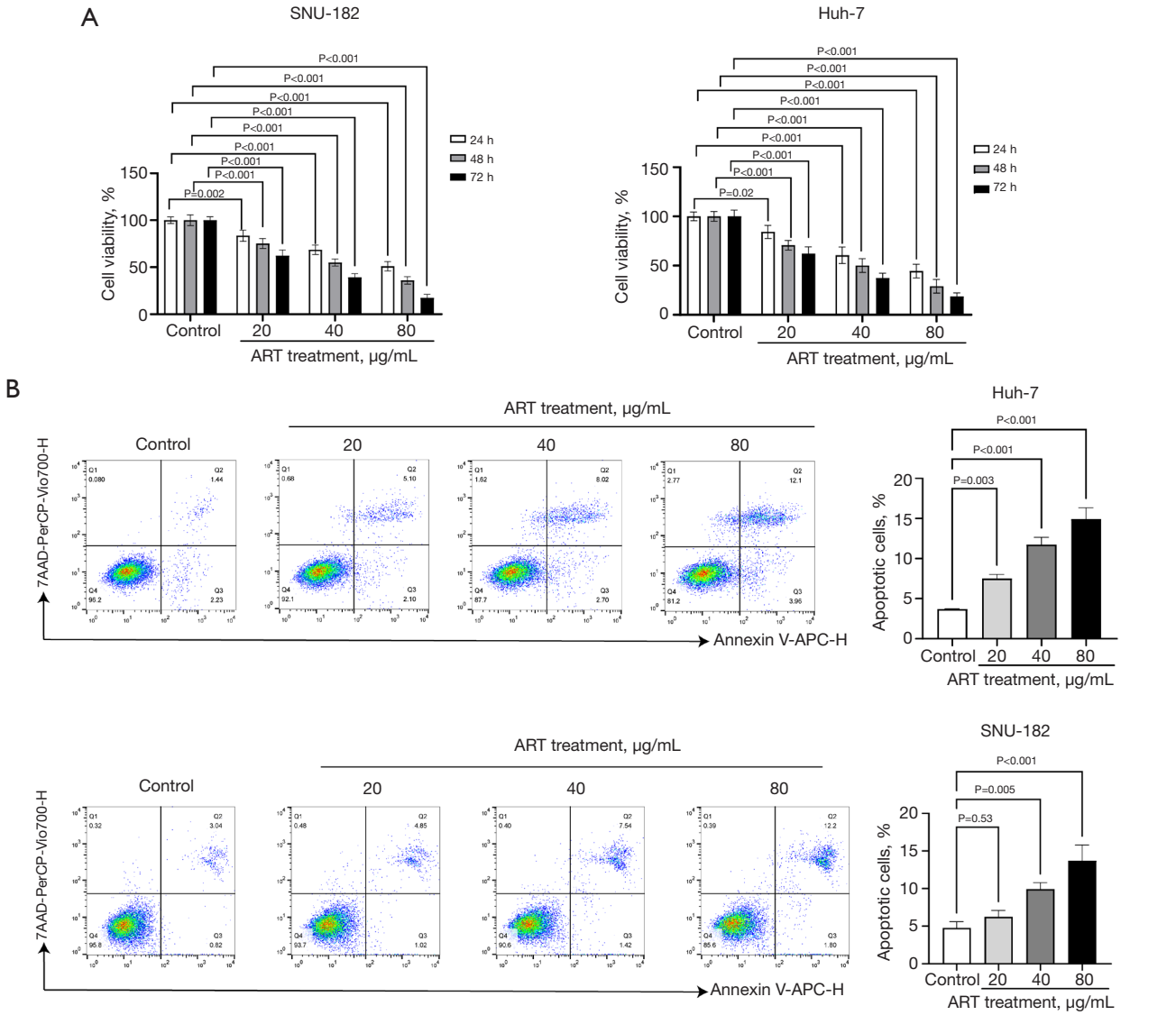

Figure 3 ART could inhibit the proliferation ability of hepatoma Huh-7 and SNU-182 cells and induce the apoptosis of Huh-7 and SNU-182 cells. (A) The proliferative ability of Huh-7 and SNU-182 cells was detected by the CCK8 method at 24, 48 and 72 h under different concentrations of ART. (B) The apoptosis of Huh-7 and SNU-182 cells was detected by flow cytometry. ART, artesunate; CCK8, cell counting kit-8.

xenograft fluorescence images of nude mice (*Figure 4C*). ART reduced the expression levels of MyD88, NF-κB, TLR4, and TRAF6 proteins (*Figure 4D*). These results suggest that ART may inhibit the growth of Huh-7 cells by inhibiting the TLR4/MyD88/NF-κB signaling pathway.

ART suppressed the TLR4/MyD88/NF-κB signaling pathway

To determine whether the TLR4/MyD88/NF-κB signaling pathway is involved in ART's antitumor and antimetastatic effects, we analyzed the relative expression levels of mRNA and protein in this pathway using western blot and qPCR. The results showed that ART inhibited the relative expression levels of MyD88, NF-κB, TLR4, and TRAF6 mRNA (*Figure 5A,5B*) and protein (*Figure 5C,5D*) in Huh-7 and SNU-182 cells. The inhibition was concentration-dependent and consistent with our *in vivo* results, confirming that ART can inhibit the activity of the TLR4/

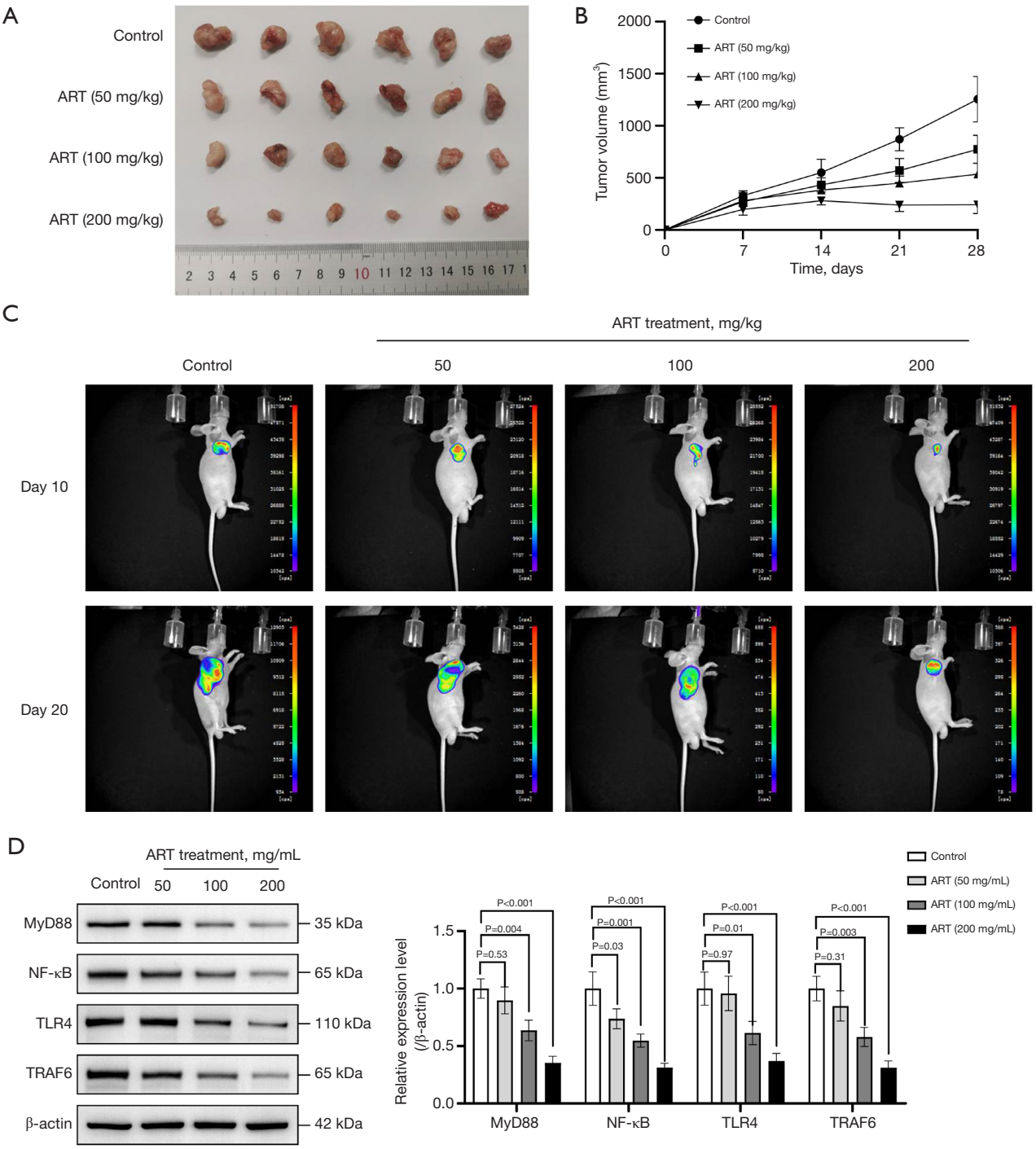

Figure 4 Effects of ART on HCC cell growth *in vivo*. (A) Schematic diagrams of the tumor sizes of tumor-bearing mice in each group after treatment with different concentrations of ART (50, 100, 200 mg/kg). (B) After treating the tumor-bearing mice as required by different groups, measure the length and width of the tumor tissues weekly for 4 consecutive weeks. Calculate the tumor volume and plot the curve of the tumor volume changing with time. (C) Fluorescent images of mice bearing Huh-7 cell xenografts were obtained on the 10th and 20th days after inoculation to observe the tumor growth in the tumor-bearing mice. (D) The relative expression levels of MyD88, NF-κB, TLR4, and TRAF6 proteins in mouse tumor tissues were detected using western blot assay. ART, artesunate; HCC, hepatocellular carcinoma; TLR4, Toll-like receptor 4; MyD88, myeloid differentiation primary response 88; TRAF6, tumor necrosis factor receptor-associated factor 6.

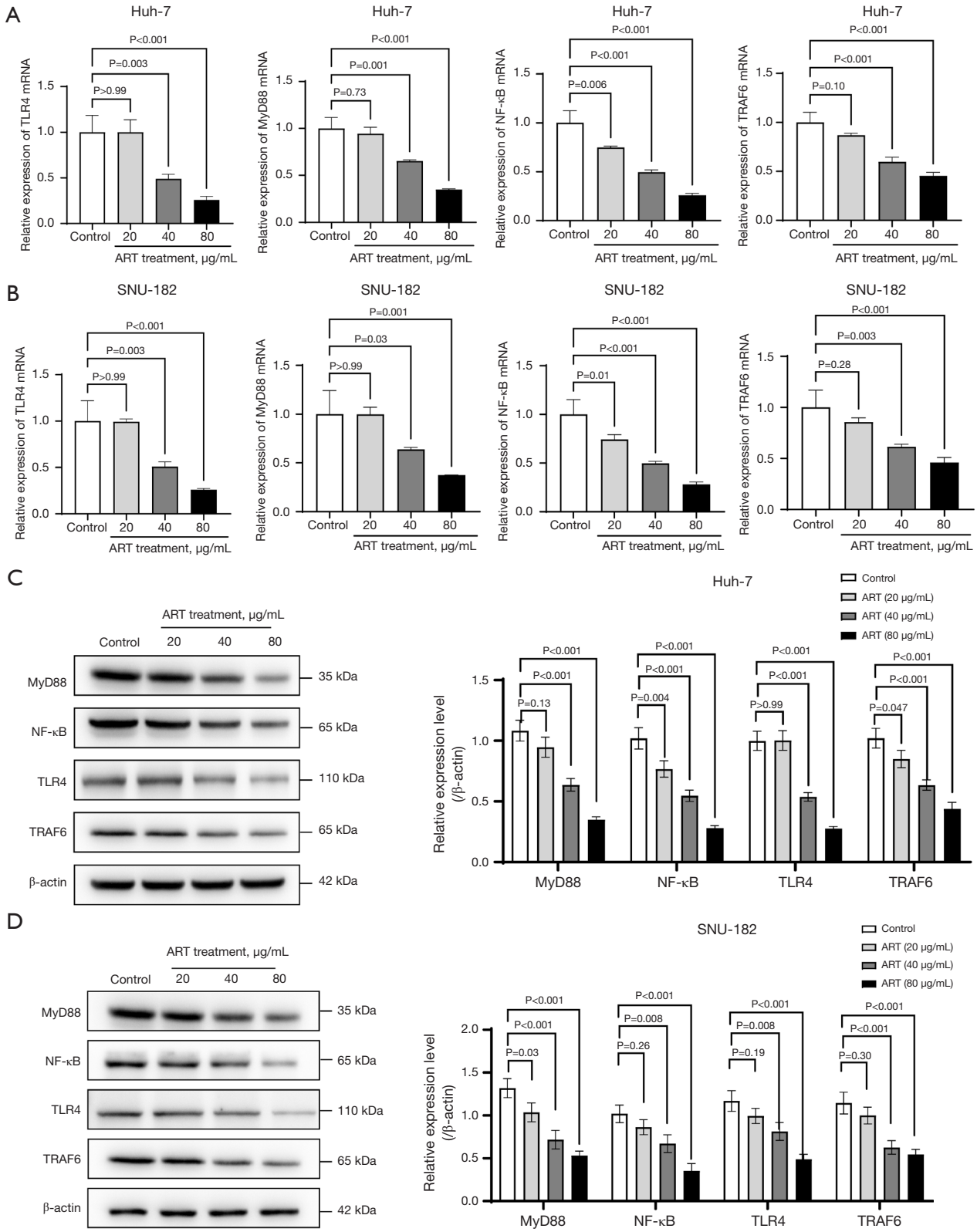

Figure 5 Effects of ART on TLR4/MyD88/NF-κB signaling pathways. (A) The mRNA expression levels of MyD88, NF-κB, TLR4, and TRAF6 in Huh-7 cells treated with ART for 48 h were detected using qPCR. (B) The mRNA expression levels of MyD88, NF-κB, TLR4,

and TRAF6 in SNU-182 cells treated with ART for 48 h were detected using qPCR. (C) The expressions of TLR4, TRAF6, MyD88, and NF-κB proteins were determined via Western blotting of Huh-7. (D) The expressions of TLR4, TRAF6, MyD88, and NF-κB proteins were determined via the Western blotting of SNU-182 cells. ART, artesunate; MyD88, myeloid differentiation primary response 88; NF, nuclear factor; qPCR, quantitative polymerase chain reaction; TLR4, Toll-like receptor 4; TRAF6, tumor necrosis factor receptor-associated factor 6.

MyD88/NF-κB signaling pathway.

ART inhibited LPS-stimulated Huh-7 cell viability

LPS, an activator of TLR4, was used to increase the levels of TLR4, IL-1β, TNF-α, and nitrite (31). In this study, Huh-7 and SNU-182 cells were treated with different concentrations of ART (40 or 80 μg/mL) and 10 μg/mL of LPS for 72 h. Our results showed that different concentrations of ART dramatically reduced the viability of LPS-stimulated Huh-7 and SNU-182 cells (*Figure 6A*). Western blot results confirmed that LPS could enhance the relative expression of MyD88, NF-κB, TLR4, and TRAF6 proteins and activate the TLR4/MyD88/NF-κB signaling pathway; meanwhile, ART could inhibit the abnormal activation of the TLR4/MyD88/NF-κB pathway. Our results further confirm that ART can inhibit the TLR4/MyD88/NF-κB signaling pathway, thereby inhibiting the proliferation of liver cancer cells (*Figure 6B*,*6C*). The mechanism of ART action is illustrated in *Figure* 7.

Discussion

ART is closely associated with the biological processes of tumorigenesis and development. However, the specific effects of ART and the mechanisms through which it affects HCC development remain unknown (32).

Previous studies have suggested that ART can induce apoptosis and autophagy in colon and bladder cancer cells (17,33) and can suppress prostate cancer cells (34). For HCC, one study found that ART decreases cell viability and tumor angiogenesis while enhancing the anticancer effects of sorafenib (13). Another study reported that ART exerts anticancer effects by inhibiting STAT-3 signaling in HCC (35). Consistent with these findings, we found that ART effectively and significantly suppressed the viability of Huh-7 and SNU-182 cells in a dose- and time-dependent manner. Additionally, ART decreased clonogenic survival, inhibited migration and invasion, and increased apoptosis in Huh-7 HCC cells. *In vivo*, it inhibited the growth of Huh-7 cell xenografts. Our research indicates that the IC_{50} value of Huh-7 is 49.18 μg/mL, that of SNU-182 is 46.11 μg/mL, and that of HepG2 is 73.62 μg/mL. We also took note of the IC_{50} values of HCC treated with ART reported by other researchers. The study by Ye *et al.* reported that the IC_{50} of Huh-7 is greater than 38.442 μg/mL (36), and according to the report by Li *et al.* (13), the IC_{50} of SNU-182 is greater than 19.221 μg/mL. Specific values for neither SNU-182 nor Huh-7 were reported, yet our IC_{50} values fall within the reported ranges. Chen *et al.* reported an IC_{50} of 14.754 μg/mL for HepG2, which significantly differs from our research result (37). He also reported that the IC_{50} of HepG2 is less than 38.442 μg/mL (11). We suspect that the inconsistency in IC_{50} values might be caused by factors such as the experimental environment, cell line type, and operational techniques. These results indicate that ART is a promising therapeutic drug for liver cancer. In addition to the observed anti-proliferative effects of ART on HCC cells, it is important to contextualize these findings within the current landscape of HCC therapies. Anti-angiogenic agents, such as sorafenib, lenvatinib, regorafenib, and cabozantinib, have been widely used in HCC treatment due to their ability to inhibit tumor angiogenesis and progression (6,38-40). While these agents have demonstrated clinical benefits, their efficacy is often limited by drug resistance and adverse effects. In contrast, ART offers a non-invasive approach with the potential to directly target tumor cells and induce apoptosis. Furthermore, a recent study has highlighted the efficacy and safety of capecitabine, an oral prodrug of 5-Fluorouracil, which exerts its cytotoxic effects primarily through the inhibition of thymidylate synthase (41). Given its distinct mechanism of action, capecitabine may serve as a promising synergistic agent to enhance the anti-tumor effects of ART. The combination of ART with capecitabine could potentially target multiple pathways involved in HCC proliferation and survival, offering a novel therapeutic strategy. Future studies should explore this combination to evaluate its synergistic potential and optimize treatment outcomes for HCC patients.

The TLR4/MyD88/NF-κB signaling pathway has been shown to induce liver inflammation and aggravate progression toward HCC (42). A recent study has reported that the expression of TLR4, MyD88, and NF-

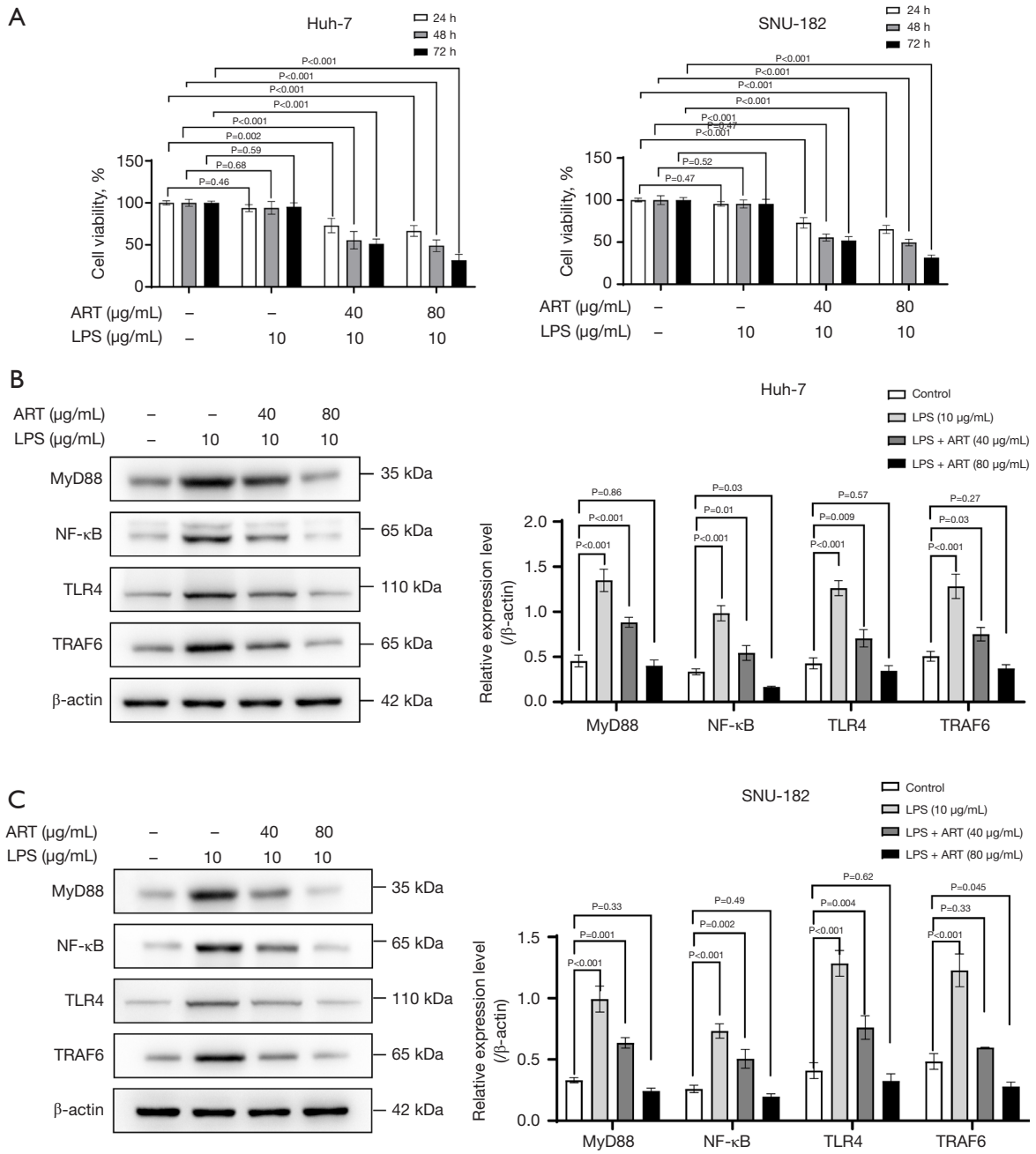

Figure 6 Effects of ART on cell viability and TLR4/MyD88/NF-κB signaling pathways in LPS-stimulated Huh-7 cells. (A) The effect of CCK8 on Huh-7 and SNU-182 cell viability after LPS or ART treatment for 24, 48, and 72 h was detected. (B) A western blot assay detected the expression of TLR4, TRAF6, MyD88, and NF-κB proteins in Huh-7. (C) A Western blot assay detected the expression of TLR4, TRAF6, MyD88, and NF-κB proteins in SNU-182. ART, artesunate; LPS, lipopolysaccharide; MyD88, myeloid differentiation primary response 88; NF, nuclear factor; TLR4, Toll-like receptor 4; TRAF6, tumor necrosis factor receptor-associated factor 6.

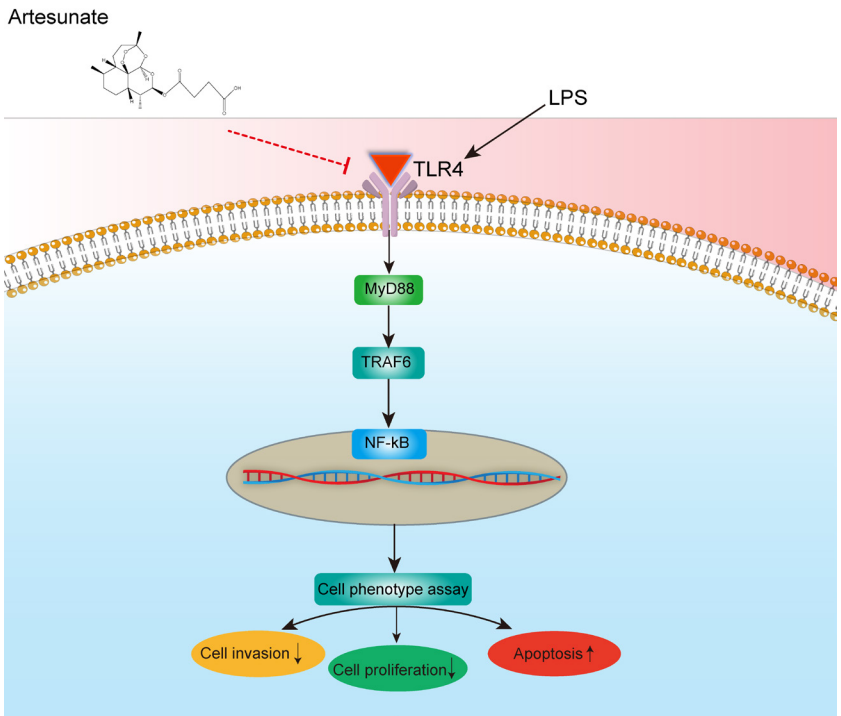

Figure 7 Mechanism by which ART inhibits hepatocellular carcinoma cells. LPS could activate the TLR4/MyD88/NF-κB signaling pathway in hepatocellular carcinoma. ART could inhibit the TLR4/MyD88/NF-κB signaling pathway, thereby inhibiting proliferation, invasion, and migration and inducing apoptosis in hepatocellular carcinoma cells. ART, artesunate; LPS, lipopolysaccharide; MyD88, myeloid differentiation primary response 88; NF, nuclear factor; TLR4, Toll-like receptor 4; TRAF6, tumor necrosis factor receptor-associated factor 6.

κB proteins was higher in HCC than in normal liver tissues, and the expression levels were correlated with poor patient survival (43). Furthermore, a study has shown that inhibiting the TLR4/MyD88/NF-κB signaling pathway suppresses the initiation and progression of HCC (44). Consistent with these previous studies, we found that ART decreased TLR4, TRAF6, MyD88, and NF-κB levels in HCC cells. The fact that ART obviously inhibited cell viability and the TLR4/MyD88/NF-κB signaling pathway in LPS-stimulated Huh-7 cells implies that ART effectively exerts anti-HCC effects through the TLR4/MyD88/NF-κB signaling pathway. Overactivation of the TLR4/MyD88/NF-κB signaling pathway may cause immune response dysfunction, resulting in tumorigenesis (45). Alterations in gene expression following ART treatment may be one of the major causes of why ART inhibits HCC progression. Our most significant result demonstrated that ART inhibits TLR4/MyD88/NF-κB signaling activity, inhibiting liver cancer cell progression.

Although our results are reassuring, there were several limitations that should be acknowledged. First, we did not include TLR4/MyD88/NF-κB pathway inhibitors to support our conclusion. Second, the safety and reliability of ART must be verified through additional *in vivo* experiments. In addition, in the experimental design of this study, no positive drug group was set up for comparison with ART. This omission poses certain challenges to the comprehensive and accurate evaluation of the efficacy of ART. Therefore, establishing a positive drug group and conducting comparative studies with ART will be one of the key directions of our follow-up research. It is important to note that this study did not include a direct comparison of ART with tyrosine kinase inhibitors (TKIs) such as sorafenib or lenvatinib, which are well-established anti-proliferative agents for HCC. Future studies should aim to compare the efficacy of ART with these agents to further elucidate its potential therapeutic role in HCC treatment. Finally, ART showed good anticancer efficacy; however, its action *in vivo* is complex and needs further confirmation by follow-up studies.

Conclusions

In conclusion, ART exhibited potent effects on the development of HCC, the underlying mechanism of which may be the alteration of the TLR4/MyD88/NF-κB signaling pathway. Thus, ART may be a potential therapeutic agent.

Acknowledgments

English language editing of this article was provided by Journal Prep Services.

Footnote

Reporting Checklist: The authors have completed the ARRIVE and MDAR reporting checklists. Available at https://jgo.amegroups.com/article/view/10.21037/jgo-2025-95/rc

Data Sharing Statement: Available at https://jgo.amegroups.com/article/view/10.21037/jgo-2025-95/dss

Peer Review File: Available at https://jgo.amegroups.com/article/view/10.21037/jgo-2025-95/prf

Funding: None.

Conflicts of Interest: All authors have completed the ICMJE uniform disclosure form (available at https://jgo.amegroups.com/article/view/10.21037/jgo-2025-95/coif). The authors have no conflicts of interest to declare.

Ethical Statement: The authors are accountable for all aspects of the work in ensuring that questions related to the accuracy or integrity of any part of the work are appropriately investigated and resolved. Experiments were carried out under a project license (No. 2021028; approval date: July 21, 2021) granted by the Institutional Animal Care and Ethics Committee of the Fourth Hospital of Hebei Medical University. These experiments complied with the "Regulations on the Administration of Laboratory Animals" and the "Guidelines for the Review of Laboratory Animal Welfare and Ethics" issued by the Ministry of Science and Technology of the People's Republic of China for the care and use of animals.

References

1. Bray F, Ferlay J, Soerjomataram I, et al. Global cancer statistics 2018: GLOBOCAN estimates of incidence and mortality worldwide for 36 cancers in 185 countries. CA Cancer J Clin 2018;68:394-424.
2. Llovet JM, Kelley RK, Villanueva A, et al. Hepatocellular carcinoma. Nat Rev Dis Primers 2021;7:6.
3. Giannini EG, Farinati F, Ciccarese F, et al. Prognosis of untreated hepatocellular carcinoma. Hepatology 2015;61:184-90.
4. Qin S, Chan SL, Gu S, et al. Camrelizumab plus rivoceranib versus sorafenib as first-line therapy for unresectable hepatocellular carcinoma (CARES-310): a randomised, open-label, international phase 3 study. Lancet 2023;402:1133-46.
5. Xia S, Pan Y, Liang Y, et al. The microenvironmental and metabolic aspects of sorafenib resistance in hepatocellular carcinoma. EBioMedicine 2020;51:102610.
6. Tang W, Chen Z, Zhang W, et al. The mechanisms of sorafenib resistance in hepatocellular carcinoma: theoretical basis and therapeutic aspects. Signal Transduct Target Ther 2020;5:87.
7. Cooper AJ, Sequist LV, Lin JJ. Third-generation EGFR and ALK inhibitors: mechanisms of resistance and management. Nat Rev Clin Oncol 2022;19:499-514.
8. Johnson M, Garassino MC, Mok T, et al. Treatment strategies and outcomes for patients with EGFR-mutant non-small cell lung cancer resistant to EGFR tyrosine kinase inhibitors: Focus on novel therapies. Lung Cancer 2022;170:41-51.
9. Luo H, Vong CT, Chen H, et al. Naturally occurring anti-cancer compounds: shining from Chinese herbal medicine. Chin Med 2019;14:48.
10. Liu M, Li H, Guo R, et al. The inhibitory effect of apatinib on different small cell lung cancer cells and in lung cancer-bearing mice and patients. Clin Respir J 2024;18:e13738.
11. He W, Huang X, Berges BK, et al. Artesunate Regulates

Neurite Outgrowth Inhibitor Protein B Receptor to Overcome Resistance to Sorafenib in Hepatocellular Carcinoma Cells. Front Pharmacol 2021;12:615889.
12. Huang Z, Gan S, Zhuang X, et al. Artesunate Inhibits the Cell Growth in Colorectal Cancer by Promoting ROS-Dependent Cell Senescence and Autophagy. Cells 2022;11:2472.
13. Li ZJ, Dai HQ, Huang XW, et al. Artesunate synergizes with sorafenib to induce ferroptosis in hepatocellular carcinoma. Acta Pharmacol Sin 2021;42:301-10.
14. Xu Z, Liu X, Zhuang D. Artesunate inhibits proliferation, migration, and invasion of thyroid cancer cells by regulating the PI3K/AKT/FKHR pathway. Biochem Cell Biol 2022;100:85-92.
15. Chen M, Wu HL, Wong TS, et al. Combination of Wogonin and Artesunate Exhibits Synergistic anti-Hepatocellular Carcinoma Effect by Increasing DNA-Damage-Inducible Alpha, Tumor Necrosis Factor α and Tumor Necrosis Factor Receptor-Associated Factor 3-mediated Apoptosis. Front Pharmacol 2021;12:657080.
16. Kurmanova A, Urazbayeva G, Salimbayeva D, et al. The relationship between Toll-like receptor-4 genes and preeclampsia outcomes. J Assist Reprod Genet 2024;41:1917-23.
17. Zhao F, Vakhrusheva O, Markowitsch SD, et al. Artesunate Impairs Growth in Cisplatin-Resistant Bladder Cancer Cells by Cell Cycle Arrest, Apoptosis and Autophagy Induction. Cells 2020;9:2643.
18. Li M, Liu J, Bi Y, et al. Potential Medications or Compounds Acting on Toll-like Receptors in Cerebral Ischemia. Curr Neuropharmacol 2018;16:160-75.
19. Yu H, Lin L, Zhang Z, et al. Targeting NF-κB pathway for the therapy of diseases: mechanism and clinical study. Signal Transduct Target Ther 2020;5:209.
20. Gao S, Chen T, Li L, et al. Hypoxia-Inducible Ubiquitin Specific Peptidase 13 Contributes to Tumor Growth and Metastasis via Enhancing the Toll-Like Receptor 4/Myeloid Differentiation Primary Response Gene 88/Nuclear Factor-κB Pathway in Hepatocellular Carcinoma. Front Cell Dev Biol 2020;8:587389.
21. Ding YF, Peng ZX, Ding L, et al. Baishouwu Extract Suppresses the Development of Hepatocellular Carcinoma via TLR4/MyD88/NF-κB Pathway. Front Pharmacol 2019;10:389.
22. Zeng XZ, Zhang YY, Yang Q, et al. Artesunate attenuates LPS-induced osteoclastogenesis by suppressing TLR4/TRAF6 and PLCγ1-Ca(2+)-NFATc1 signaling pathway. Acta Pharmacol Sin 2020;41:229-36.
23. Chen Y, Wu J, Zhu J, et al. Artesunate Provides Neuroprotection against Cerebral Ischemia-Reperfusion Injury via the TLR-4/NF-κB Pathway in Rats. Biol Pharm Bull 2021;44:350-6.
24. Kim S, Park J, Han J, et al. Hepatitis B Virus X Protein Induces Reactive Oxygen Species Generation via Activation of p53 in Human Hepatoma Cells. Biomolecules 2024;14:1201.
25. López-Terrada D, Cheung SW, Finegold MJ, et al. Hep G2 is a hepatoblastoma-derived cell line. Hum Pathol 2009;40:1512-5.
26. Heo Y, Jeong H, Yoo Y, et al. Structural and Functional Characterizations of Cancer Targeting Nanoparticles Based on Hepatitis B Virus Capsid. Int J Mol Sci 2021;22:9140.
27. Wu Z, Shi Y, Ren S, et al. ADAMTS8 Inhibits Progression of Esophageal Squamous Cell Carcinoma. DNA Cell Biol 2020. [Epub ahead of print]. doi: 10.1089/dna.2020.6053.
28. Riccardi C, Nicoletti I. Analysis of apoptosis by propidium iodide staining and flow cytometry. Nat Protoc 2006;1:1458-61.
29. Liu L, Cui S, Zhang R, et al. MiR-421 inhibits the malignant phenotype in glioma by directly targeting MEF2D. Am J Cancer Res 2017;7:857-68.
30. Pillai-Kastoori L, Schutz-Geschwender AR, Harford JA. A systematic approach to quantitative Western blot analysis. Anal Biochem 2020;593:113608.
31. Ma L, Feng L, Ding X, et al. Effect of TLR4 on the growth of SiHa human cervical cancer cells via the MyD88-TRAF6-TAK1 and NF-κB-cyclin D1-STAT3 signaling pathways. Oncol Lett 2018;15:3965-70.
32. Ruwizhi N, Maseko RB, Aderibigbe BA. Recent Advances in the Therapeutic Efficacy of Artesunate. Pharmaceutics 2022;14:504.
33. Ma QY, Liu YC, Zhang Q, et al. Integrating network pharmacology, molecular docking and experimental verification to reveal the mechanism of artesunate in inhibiting choroidal melanoma. Front Pharmacol 2024;15:1448381.
34. Wang Z, Wang C, Wu Z, et al. Artesunate Suppresses the Growth of Prostatic Cancer Cells through Inhibiting Androgen Receptor. Biol Pharm Bull 2017;40:479-85.
35. Ilamathi M, Santhosh S, Sivaramakrishnan V. Artesunate as an Anti-Cancer Agent Targets Stat-3 and Favorably Suppresses Hepatocellular Carcinoma. Curr Top Med Chem 2016;16:2453-63.
36. Ye RR, Peng W, Chen BC, et al. Mitochondria-targeted artesunate conjugated cyclometalated iridium(iii)

complexes as potent anti-HepG2 hepatocellular carcinoma agents. Metallomics 2020;12:1131-41.
37. Chen W, Ma Z, Yu L, et al. Preclinical investigation of artesunate as a therapeutic agent for hepatocellular carcinoma via impairment of glucosylceramidase-mediated autophagic degradation. Exp Mol Med 2022;54:1536-48.
38. Yi C, Chen L, Lin Z, et al. Lenvatinib Targets FGF Receptor 4 to Enhance Antitumor Immune Response of Anti-Programmed Cell Death-1 in HCC. Hepatology 2021;74:2544-60.
39. Deng S, Solinas A, Calvisi DF. Cabozantinib for HCC Treatment, From Clinical Back to Experimental Models. Front Oncol 2021;11:756672.
40. Granito A, Marinelli S, Forgione A, et al. Regorafenib Combined with Other Systemic Therapies: Exploring Promising Therapeutic Combinations in HCC. J Hepatocell Carcinoma 2021;8:477-92.
41. Granito A, Marinelli S, Terzi E, et al. Metronomic capecitabine as second-line treatment in hepatocellular carcinoma after sorafenib failure. Dig Liver Dis 2015;47:518-22.
42. Hassan HM, Al-Wahaibi LH, Shehatou GS, et al. Adamantane-linked isothiourea derivatives suppress the growth of experimental hepatocellular carcinoma via inhibition of TLR4-MyD88-NF-κB signaling. Am J Cancer Res 2021;11:350-69.
43. Lupi LA, Cucielo MS, Silveira HS, et al. The role of Toll-like receptor 4 signaling pathway in ovarian, cervical, and endometrial cancers. Life Sci 2020;247:117435.
44. Vandewynckel YP, Laukens D, Geerts A, et al. Therapeutic effects of artesunate in hepatocellular carcinoma: repurposing an ancient antimalarial agent. Eur J Gastroenterol Hepatol 2014;26:861-70.
45. Chen S, Yu W, Zhang K, et al. Comparison of the efficacy and safety of Transarterial chemoembolization with and without Apatinib for the treatment of BCLC stage C hepatocellular carcinoma. BMC Cancer 2018;18:1131.

Cite this article as: Wu Y, Wu J, Li Z, Wu Z, Li S, Yang G, Rong X, Wang Q, Li Y, Xia Q, Shi G. Inhibition of hepatocellular carcinoma progression by artesunate via modulation of the TLR4/MyD88/NF-κB signaling pathway. J Gastrointest Oncol 2025;16(2):599-614. doi: 10.21037/jgo-2025-95